The Mount Cameroon southwest flank eruptions: Geochemical constraints on the subsurface magma plumbing system

Caroline Neh Ngwa[1, 2,*], Nils Lenhardt[2], Petrus le Roux[3], Benoît Joseph Mbassa[1]

[1]Mount Cameroon Observatory, Institute for Geological and Mining Research, P.O. Box 370 Buea, SW Region, Cameroon

[2]University of Pretoria, Department of Geology, Private Bag X20, Hatfield, 0028 Pretoria, South Africa

[3]University of Cape Town, Department of Geological Sciences, Private Bag X3, 7701 Rondebosch, South Africa

* Corresponding author

Highlights

- Sr isotope ratios for the 1999 samples are somewhat different than limits so far obtained for previous Mt. Cameroon lavas.
- Bulk rock element trends indicate fractional crystallization, while disequilibrium textures indicate magma mixing/recharge.
- Plots of K2O and Nb show a mixing trend between samples from these three eruptions implying a common magma chamber
- Clinopyroxene geobarometric calculations show common dominant crystallisation depth at 23-29 km for these samples.

Abstract

With seven major eruptions in the 20th century, Mount Cameroon is one of the most active volcanoes in Africa. However, information on the volcano's plumbing system is still relatively scarce. In order to contribute to filling this knowledge gap, a geochemical, clinopyroxene geobarometry, and Sr-Nd isotope study was carried out on samples collected from the 1922 and lower 1999 lava flows found on the SW flank of the volcano. Petrographic evidence shows a common crystallising mineral assemblage of olivine and clinopyroxene and/or plagioclase scattered in a microlite-rich groundmass. Total alkali-silica classification diagram shows that the lavas of 1922 exhibit basanitic compositions and those of 1999 mostly basanitic with some literature data as hawaiites. The Sr isotope ratios for the 1999 samples in this study show values somewhat lower and higher than the limits obtained so far for historic Mount Cameroon samples. While major and trace element trends indicate fractional crystallization processes, chemical and mineral disequilibrium textures are indicative of open-system processes such as magma mixing and magma chamber recharge. Variations in incompatible trace element ratios, which hardly change during fractional crystallisation are also suggestive of open-system processes. Plots of K_2O and Nb show a mixing trend between samples from these eruptions implying a common magma chamber where remnant material from preceding eruptions was incorporated into succeeding eruptions. Clinopyroxene geobarometric calculations show this common dominant crystallisation depth at 23-29 km.

Keywords: Mount Cameroon; flank eruptions; magma chamber processes, crystallisation depths

1. Introduction

Located at 4.20°N, 9.17°E, Mount Cameroon (volcano number 224010; Global Volcanism Program, 2013) is an elliptical stratovolcano with a height of approximately 4095 m above sea level and a volume of ca. 1200 km^3 (Suh et al., 2003). Eruptions at Mount Cameroon are characterized by vent-clearing explosive events with the emission of ash clouds and pyroclastic falls, followed by the effusion of mafic lava along fissures. These eruptive activities extend back to about 3 million years (Wandji et al., 2009). The earliest well-authenticated eruption, however, was in 1909 (Fitton et al., 1983). Prehistoric eruptions that occurred before the authenticated period are represented by alternating lava flows and pyroclastic deposits in addition to pyroclastic cones, which are scattered all over the volcano. In recent times (since the 20th century), there have been seven significant eruptions at Mount Cameroon, making it one of the most active volcanoes in Africa (Lenhardt and Oppenheimer, 2014). These seven eruptions (Fig. 1a) took place in 1909 with an eruption on the northeast flank of the volcano, in 1922 with combined summit activity and lava emission on the south-western flank, in 1954 with strombolian explosive activity at the summit, and in 1959 with eruptions from three vents on the north-eastern flank of the volcano. Further activity occurred in 1982 and 1999 with eruptions on the south-western flank, and lastly, in 2000 with a summit eruption. All these eruptions resulted in the production of lava flows and/or pyroclastic materials. The total volume of lava for these seven eruptions is estimated to be $3 – 10 \times 10^3$ m^3 (Suh et al., 2003).

Geochemical investigations on Mount Cameroon have addressed these recent eruptions individually or collectively. For instance, Fitton et al. (1983) noted that variations in the 1982 lavas resulted from the mixing of more mafic magma with a residual magma in a sub-volcanic chamber. Déruelle et al. (1987) showed that fractional crystallization of olivine, clinopyroxene, and Fe–Ti oxides is the dominant process controlling the overall differentiation of the Mount Cameroon magma suite. According to Déruelle et al. (2000) there is a unique magmatic reservoir, inside which the magma differentiation takes place by crystal settling of denser mineral phases. Njome et al. (2008) proposed that each of the recent eruptions is not fed from this single large evolving chamber, but by discrete batches of magma from different storage regions, which erupt independently.

Despite these former works, knowledge of the volcano's internal system is still scarce. Specifically, understanding the magma evolutionary processes along with magma crystallisation depths are needed in order to support monitoring and early warning systems for hazard mitigation strategies in this area. This is very important because the flanks of this volcano are densely populated by ≥ 0.5 million people (Thierry et al., 2008), who are

attracted to the region by its fertile soil and the associated economic activities. Being a large volcano with eruptions recognised to occur either at the summit and/or along its NE-SW flanks, there is still a knowledge gap regarding whether magma for these sectorial eruptions are supplied from a common magma chamber or not. In response, we present in this contribution, a geochemical, clinopyroxene (cpx) geobarometry, and Sr-Nd isotope study performed on samples collected from both 1922 and 1999 lava flows found on the SW flank of the volcano. We integrate and compare these data with literature data on the 1982 lavas in order to enhance understanding of the dynamics of the magma feeding eruptions on this flank of Mount Cameroon.

2. Geological Setting

Mount Cameroon forms part of the Cameroon Volcanic Line (CVL, Fig. 1b), which is a prominent intraplate alignment of 12 Cenozoic volcanoes and/or volcanic centers in West Africa. The CVL runs for approximately 1600 km from the island of Annobon in the Gulf of Guinea through Cameroon to the Biu Plateau in northeastern Nigeria. The associated volcanoes/volcanic centers include Annobon, São Tomé, Principe, and Bioko, in the oceanic sector; and Mounts Cameroon, Etinde, Manengouba, Bambouto, Oku Mountains, Ngaoundéré Plateau, Mandara Mountains, and the Biu Plateaux in the continental sector. The Mandara Mountains (32 Ma) are the oldest of these volcanic centers (Fitton and Dunlop 1985), while Mount Cameroon, situated midway in the CVL, is presently the most active volcano with its most recent eruption in the year 2000. Recent geochronological data (Moundi et al., 2007), however, reveal that the oldest volcanic ages (K-Ar) so far obtained for the CVL are from transitional lavas (51.8±1.2 Ma) and olivine basalt (46.7±1.1 Ma) in the Bamoun Plateau.

The basement of the continental sector of the CVL is composed of Pan-African schists and gneisses, which have been intruded by syenite and granitoid ring complexes less than 70 million years ago (Toteu, 1990; Toteu et al., 1994). The basement of the oceanic volcanic centers varies in depth from 4 km in Pagalu, to 0.5 km in Bioko. Pagalu is built directly upon the oceanic crust (Gorini and Bryan 1976). Sao Tome and Principe are on Cretaceous sediments (Hedberg 1968) while Bioko is built upon the African continental shelf (in Déruelle et al., 1987).

Magmatic rocks on the CVL range from ultrabasic-basic to strongly evolved, and dominantly alkaline to rare sub alkaline. The ultrabasic-basic rocks have generally similar major and trace element compositions, suggesting similar sub-lithospheric mantle sources for

both continental and oceanic magmas (Fitton and Dunlop, 1985). Geochemical-isotopic investigations on the mantle source of CVL magmas (Aka et al., 2004; Halliday et al., 1988, 1990; Lee et al., 1994) suggest the involvement of a depleted (DM) and a high U/Pb (HIMU) or FOZO mantle. Many other studies on geochemical and petrologic investigations (e.g., Merle et al., 2017; Kamgang et al., 2008; Yokoyama et al., 2007, Marzoli et al., 2000, Rankenburg et al., 2005) have shown evidence for the involvement of both the sub-continental lithospheric mantle (SCLM) and the crust in the origin of the CVL magmas.

Although rocks from the CVL volcanoes show geochemical and radiogenic isotope characteristics that are typical of plume activity, unlike typical hotspot settings, there is the lack of an age progression when migrating from one volcano to another (Fitton and Dunlop, 1985; Aka et al., 2018). This unique characteristic of the CVL has led to the generation of numerous models (ranging from plumes, structural, geochemical-isotopic, and geophysical) regarding its origin. Some of these models evoke single (Morgan, 1983) or multiple (Ngako et al., 2006) mantle plumes. Ebinger and Sleep (1998), propose that pre-existing lithospheric structures control the formation of the CVL. Many other proposed models (King and Anderson, 1995, 1998; Meyers et al., 1998; King and Ritsema, 2000) for the CVL formation rely on convection driven by various forces. Shellnutt et al. (2016), put forward shear zone reactivation, leading to ‘leaking’ of mantle-derived material through pre-existing lithospheric structures. Geochemical and isotopic investigations (Aka et al., 2004; Halliday et al., 1988; Halliday et al., 1990; Lee et al., 1994) suggest the involvement of a depleted (DM) and a high U/Pb (HIMU) or FOZO mantle

The tectonics along the CVL are discernible by two major directions: (1) the N20–40°E direction, which is that of the volcanic line along which several parallel and transversal fractures are buried by lava flows (Moreau et al., 1987), and (2) the N70°E direction, which corresponds to a major Precambrian shear zone considered as the continuation of the Pernambuco lineament in the northeast of Brazil, and prior to the continental separation (Browne and Fairhead, 1983; Burke et al., 1971; Ngako et al., 2003).

3. Sampling and analytical methods

A total of 14 samples (six from the 1922 and eight from the 1999 lava flows) were collected for petrographical and geochemical analyses. Preparation of samples and sample analyses were carried out using standard methods after Loubser and Verryn (2008). Bulk major element analyses were done on fused beads using the Thermo Fisher ARL Perform'X Sequential XRF instrument with OXSAS software at the University of Pretoria, South Africa. The certified

reference material SARM 49 and blanks were analysed with each batch of samples for accuracy and quality control. Another aliquot of each sample was pressed in a powder briquette to determine some trace elements.

Trace and rare earth elements (REE) were determined using the Thermo XSeries II inductively coupled plasma mass spectrometry (ICP-MS) at the University of Cape Town. Sr and Nd isotope analyses were done using a Nu Instruments NuPlasma HR MC-ICP-MS at the University of Cape Town, following elemental separation chemistry. Details of the chemical sample preparation and instrumental analysis techniques are the same as reported in Harris et al. (2018). The international reference material BHVO-2 was processed as unknown with these samples for quality control during these analyses, and results agree with the excepted values for this reference material in the GeoRem database.

Microprobe analyses of clinopyroxene phenocrysts were conducted at the University of Cape Town using a JEOL Superprobe JXA-8100 electron microprobe equipped with four wavelength dispersive spectrometers, a range of crystals (LDE1, LDE2, PETJ, PETH, TAP, LIF, LIFH), fitted with two gas-flow proportional and two sealed Xenon detectors. The electron beam was set to an accelerating potential of 15 kV, a beam current of 20 nA, and a 1-3 μm diameter. Measurements were performed with counting times of 10 seconds on peak and 2 x 5 seconds on background.

4. Results

4.1. Petrography

The 1922 samples range from aphyritic to porphyritic. The porphyritic samples with 5-30 vol. % of phenocrysts, predominantly consist of olivine and clinopyroxene. Phenocrysts (≥ 0.3 mm) are either euhedral or very fragmented and embayed. Resorption textures (Fig. 2c, d) are common in the phenocrysts, which are indications of textural disequilibrium during evolution. Scarce clusters of microphenocrysts also occur. Most olivines are round or subrounded in outline with scarce euhedral crystals (Fig. 2e). Clinopyroxene phenocrysts occur either individually or in clusters with some melt inclusions or opaque minerals. Clinopyroxene phenocrysts show several zonation patterns in Back-Scattered Electron (BSE) images (Fig. 2b). The groundmass, however, is similar in all samples and made of a fine-grained to a glassy matrix with needle-like microlites of plagioclase, diopside, olivine, Fe-Ti oxides in addition to volcanic glass.

The 1999 lavas are all porphyritic, displaying more than 10 vol. % phenocrysts and showing heterogeneous textures. The phenocrysts (≥0.3 mm) are composed of olivine and

clinopyroxenes while the microphenocrysts (<0.3 mm) and microlites (≤0.03 mm) are composed of olivine, clinopyroxene, plagioclase, and Fe-Ti oxides. The olivine phenocrysts are prismatic and euhedral to anhedral in outline. Clinopyroxene phenocrysts and microphenocrysts are typically twinned, and octahedral to euhedral in outline. Clinopyroxenes with corroded and serrated margins and embayed structures also occur. Scarce melt and opaque mineral inclusions are found enclosed in the clinopyroxene phenocrysts. Like the clinopyroxene phenocrysts from the 1922 lavas, clinopyroxenes in the 1999 lavas exhibit several zoning patterns. Representative samples of zoning patterns from this study, as seen in BSE images are shown in Fig. 2a. Plagioclase occurs both as phenocrysts and microlites in these lavas. The plagioclase either occurs in isolation or as clusters of skeletal laths.

For comparison, the 1982 lavas are described as aphyric with less than 1 vol.% phenocrysts of olivine (≤4 mm) and clinopyroxenes (<4 mm), scattered in a microlite-rich groundmass (Fitton et al., 1983; Suh et al., 2003). Olivines are sub-rounded to round and embayed while the clinopyroxenes are subhedral and in most cases display oscillatory zoning (Suh et al., 2003). Furthermore, olivine microphenocrysts are elongated and arranged parallel to plagioclase microlites (Suh et al., 2003).

4.2. Geochemistry of whole rocks

Whole-rock major and trace element data for the 1922 and 1999 lavas that have been analysed for this study are presented in Table 1. The lavas of the 1922 eruption show widespread in SiO_2 (42.99-45.51 wt%) and total alkalis (4.43-6.03 wt%) compared to the 1999 lavas with SiO_2 values ranging between 43.82-45.56 wt% and total alkali values of 5.37-5.90 wt%. All plot in the basanite field on the total alkali-silica (TAS) classification diagram (Fig.3). This is in good agreement with the majority of the available literature data from the 1922 and 1982 lavas (Fitton et al., 1983, Yokoyama et al., 2007), and the 1999 lavas (Suh et al., 2003). Nevertheless, some of the literature data from the 1982 and 1999 lavas also plot into the hawaiite and basalt fields (Fig. 3).

Figure 4 presents major element scatter diagrams with each oxide plotted against MgO weight percentages (wt. %). The data from the present study are largely in agreement with literature data from these eruptions. The concentrations of major element oxides such as Na_2O, and Al_2O_3 show a negative correlation while others show a positive correlation with increasing MgO. In terms of individual eruptions, despite the fact that the 1999 samples have the most evolved rocks, major element concentrations of lavas from the 1922 samples show the widest

ranges amongst these three eruptions. This is in line with petrographic observations where the 1922 lavas range from aphyritic to porphyritic.

Figure 5 shows the trace element vs MgO variation diagrams for the analysed samples alongside literature data for representative samples of the 1982, 1922 and 1999 lavas. The concentrations of compatible trace elements (e.g., Cr and Ni) in the samples increase with increasing MgO (Fig 5a, b), suggestive of olivine and clinopyroxene crystallisation. The 1922 samples generally show the highest values of compatible trace elements. Similar to the total alkalis, major elements, and compatible trace elements, the concentrations of incompatible elements in the 1922 lavas also cover the widest range compared to the 1999 and 1982 lavas, although the 1999 lavas are more evolved. Nevertheless, the concentrations of the incompatible elements (e.g Ba and Rb) from individual eruptions show a general decreasing trend when considered together with increasing MgO (Fig. 5c, d).

4.3. Sr and Nd isotopes

The Sr and Nd isotope ratios of the samples from the 1922 eruption range from 0.70326-0.70332 and 0.51278-0.51281, respectively. The values of the 1999 lavas are 0.70309-0.70337 and 0.51278-0.51281, respectively. Previous studies on Mount Cameroon samples (e.g. Halliday et al., 1988; Fitton et al., 1983; Yokoyama et al., 2007) show that Sr and Nd isotope ratios are within the ranges of 0.70317 - 0.70333 and 0.51276 - 0.51281, respectively (Fig. 6 a). Almost all the samples from the two eruptions analysed for this study have values within this compositional range. Nevertheless, two samples from the 1999 lavas do not fit into the Sr isotope compositional range: 1) sample BkB is the least enriched in radiogenic Sr with a $^{87}Sr/^{86}Sr$ ratio of 0.70309. This value rather falls within the $^{87}Sr/^{86}Sr$ ratio range for St. Helena data ($^{87}Sr/^{86}Sr$ = 0.7028–0.7031; Stracke et al., 2003). 2) Sample BkC is the most enriched in radiogenic Sr with a $^{87}Sr/^{86}Sr$ value of 0.70337. Generally, the isotopic compositions vary within and between the lavas of the different ages. Previous work (Yokoyama et al., 2007) proposed that the isotopic variation in the Mount Cameroon samples results from the interaction of melts derived from the asthenospheric mantle with overlying sub-continental lithospheric mantle. Nevertheless, all samples plot within the HIMU mantle reservoir field of Zindler and Hart (1986), a typical characteristic of the CVL lavas (Halliday et al., 1988, 1990, Aka et al., 2004).

4.4. Clinopyroxene chemistry and thermobarometry

Microprobe analyses of clinopyroxene phenocrysts from the 1922 and 1999 lavas show a compositional range of Mg numbers [Mg# = 100*molar MgO/(MgO + FeO)] between 75 and 85.1. The clinopyroxene crystals have compositional normal zoning with higher Mg# in the cores than in the rims. Microprobe analyses of clinopyroxene phenocrysts from the 1922 and 1999 lavas are presented in Table 2. They show compositions with Mg# ranging from 75.72 to 84.92 for the 1922 samples and 76.41- 85.10 for the 1999 samples. To determine the depth of magma stagnation, thermobarometry calculations were carried out on clinopyroxene-liquid pairs using the spreadsheet of Putirka (2008) and the formulations of Putirka et al. (1996). The precision of the method for a calculation of T and P are ±30 °C and ±1.7 kbar, respectively. Using these simulations, thermobarometry is dependent on identifying a suitable liquid composition (this can be the composition of glass, or the whole rock, or some calculated composition) most likely to be in equilibrium with a given clinopyroxene. In applying this method, we used compositions of whole rocks as the nominal liquids alongside the compositions of clinopyroxene cores. The selected liquids had compositional Mg# values of 51.1 and 59.8 for the 1922 and 51.9 for the 1999 lavas. In order to ensure that the clinopyroxene compositions used for thermobarometric calculations in this study are in equilibrium with the available nominal melt compositions, we plotted the Mg# of clinopyroxene cores against the Mg# of the potential nominal melts. Crystal-liquid pairs with observed values of KD $(Fe\text{-}Mg)^{cpx\text{-}liq}$ comparable with the theoretical equilibrium value of 0.27 ± 0.03. KD $(Fe\text{-}Mg)^{cpx\text{-}liq}$ (Purtika 2008) were considered to validate equilibrium conditions (Fig. 7 a, b) and were thus used for thermobarometry calculations. For the 1922 samples, the nominal melt Mg# 51.1 was in equilibrium with clinopyroxene having Mg# less than 80 while clinopyroxenes with Mg#s above 80 were in equilibrium with the nominal melt Mg# 59.8. The calculations yielded two groups of pressures and temperatures, i.e. one group with 7-10 kbar and 1173.2-1196.3 °C, and the other with 10-12 kbar and 1235.7-1246.4^{o}C, respectively. Assuming a depth increase of 3.3 km per kbar (Putirka, 1999), these two pressure groups (7-10 kbar and 10-12 kbar) correspond to a wide range of clinopyroxene crystallisation depths from approximately 23 to 39 ± 6 km for the 1922 eruption. For the 1999 lavas, clinopyroxene crystals in equilibrium with the nominal melt exhibit an Mg# range from 77.3 to78.9. Calculated thermobarometry from these clinopyroxene-liquid pairs gave pressure and temperature ranges of 7.8-8.6 kbar and 1182.8-1188.7^{o}C, respectively. This pressure range translates to a range of clinopyroxene crystallisation depths from approximately 25.7-28.4 ± 6 km, similar to the clinopyroxene crystallization depth range of Geiger et al. (2016) for the 1999 eruption.

5. Discussion

5.1 Thermobarometry relationship

In the present study, the 1922 lavas reveal clinopyroxene crystallisation depths between 23 and 39 ± 6 km, while the 1999 lavas discloses depths of 25.7 to 28.4 km. Geiger et al. (2006) identified deep levels of crystallisation (26-39 km), recorded by plagioclase and a dominant zone of clinopyroxene crystallisation at a depth range between 20 and 28 km for the 1999 and 2000 eruptions. Consequently, we presume that the occurrence of overlapping similar crystallisation depths for the 1922 and 1999 lavas from the same flank of the mountain indicate a common magma chamber located at least around the Moho level. Geophysical data (Ateba et al., 2009) locate a magmatic conduit below the summit of Mount Cameroon during the 2000 eruption. This magmatic conduit was interpreted to be the main pass-way for magma rising from a main Moho storage zone beneath Mount Cameroon. Geochemical data (Suh et al., 2003) and thermobarometry data on Mount Cameroon rocks (Geiger et al., 2016) locate a dominant magma storage zone below the Moho level, which is found at 24 ± 2 km (Ambeh et al., 1989). This Moho-chamber is supposedly sourced by magma from deeper levels as indicated by the high depth (>30 km) of crystallisation recorded for the 1922 lavas for this study and earlier contributions (Geiger et al., 2016) for the 1999 samples. The calculated high depth corroborates the information gained from reported earthquake hypocentres at 30-55 km depth underneath Mount Cameroon preceding the 1999 and 2000 eruptions (Ngongang et al., 2019, and references therein), which were interpreted to indicate magma migration at that depth (Suh et al., 2003).

5.2. Geochemical relationships

Temporal variations of major element ratios (CaO/Al_2O_3; Fig. 8a) reveal that the 1922 lavas have large discrepancies while those of 1982 and 1999 samples are restricted. This is in agreement with petrographic observations, which show that the 1922 lavas ranged from aphyritic to porphyritic. Therefore, in line with these petrographic and geochemical observations, the variations of Ca/Al_2O_3 and compatible trace elements (not shown) in the 1922 lavas are most likely due to the variations in the content of mafic phenocrysts. Although the above observations may be linked to dissimilarities in phenocryst accumulations, the variations in incompatible trace elements, which are not taken up by the crystallising mineral phases in these lavas, cannot be attributed to mineral accumulation. Temporal variations of these elements (Fig. 8b-c) reveal that the most evolved lavas are found in 1922 and 1999 as

the lavas from these eruptions show the highest contents of incompatible elements. However, as seen in Fig. 8b-c, incompatible trace element (Rb and La) fluctuations are highest in the 1922 lavas, and least in the lavas of the 1982 eruption. The ratio of incompatible elements, which hardly changes during fractional crystallisation (Fig. 8d), shows variations between and within each eruption. This implies that, although major element and compatible trace element plots show general fractionation trends, the variation of incompatible element ratios within and between individual eruptions are indications of mixing of magma with different evolutionary levels. The scatter in the plots of 1/Sr vs $^{87}Sr/^{86}Sr$, and K_2O vs $^{87}Sr/^{86}Sr$ are also indications that mixing occurred between magmas, rather than melts, because the mixing of melts would generate good linear correlation on these diagrams. The coexistence of zoned, strongly serrated-margined, sieve-textured clinopyroxene grains, and rounded olivine phenocrysts in the same sample also indicate disequilibrium between the minerals and the host melt and suggest rapid changes in pressure, temperature or magma chemistry, as has been proposed in the case of Mt. Bambouto on the CVL (Marzoli et al., 2015) and other volcanoes (Stroncik et al., 2009; Hildner et al., 2011). Plotting 1922, 1982 and 1999 lava compositions on Nb vs. K_2O plot, reveals a mixing trend between the three compositions (Fig. 7d), implying that remnant material from preceding eruptions was incorporated into succeeding eruptions. Our barometry data highlight a common magma stagnation depth close to the Moho level where magma mixing probably occurred before ascent.

6. Conclusion

The lavas from the SW flank eruptions of Mount Cameroon are aphyritic to porphyritic, with similar mineral assemblages. The main mineral assemblage is made up of olivine, clinopyroxene ± plagioclase while the groundmass consists of a fine-grained to a glassy matrix with needle-like microlites of plagioclase and diopside, Fe-Ti oxides, and volcanic glass. The lavas contain both normally and reversely zoned clinopyroxene phenocrysts, reflecting complex magma chamber processes involving open system evolution and mixing before eruption. Plots of K_2O and Nb show a mixing trend between samples from these three eruptions, implying a common magma chamber where remnant material from preceding eruptions was incorporated into succeeding eruptions. Barometry data calculated from clinopyroxene-liquid pairs reveal a common clinopyroxene crystallisation depth at 23-28 km for the 1922 and 25.7-28.4 kbar for the 1999 eruption, where mixing of remnant and new magmas may have occurred before each eruption.

Although the present study show Sr and Nd isotope ratios which are generally in good agreement with those from previous studies, two samples from the 1999 lavas do not fit into the Sr isotope compositional range: 1) sample BkB is the least enriched in radiogenic Sr with a $^{87}Sr/^{86}Sr$ ratio of 0.70309. 2) Sample BkC is the most enriched in radiogenic Sr with a $^{87}Sr/^{86}Sr$ value of 0.70337. These observations suggest the need for further isotope studies from Mount Cameroon. Given the location of this volcanic on the CVL and the lack of crustal contamination on the eruption products, a large new isotope data set may be helpful to unravel the mantle source of the CVL mafic rocks.

Acknowledgments

The National Research Foundation of South Africa (NRF) (N.L., grant no. 90800) and the University of Pretoria are thanked for their financial support. This manuscript was written during a one-month research visit of C.N. Ngwa to the University of Pretoria. The visit was sponsored by the UNESCO-ANESI Outstanding Women in Geoscience Fellowship. Jeanette Dykstra (University of Pretoria) is thanked for providing the XRF data. Chris Harris and Nicholas Laidler (University of Cape Town) are thanked for the help with the microprobe analysis. The comments of an anonymous reviewer, Andrea Marzoli, and Aka Festus Tongwa greatly helped in improving the manuscript. We appreciate the editorial handling of Sandro Aiuppa.

References

Aka, F.T., Hasegawa, T., Nche, L.A., Asaah, A.N.E., Mimba, M.E., Teitchou, I., Ngwa, C.N, Miyabuchi, Y., Kobayashi, T., Kankeu, B., 2018. Upper Triassic mafic dykes of Lake Nyos, Cameroon (West Africa) I: K-Ar age evidence within the context of Cameroon Line magmatism, and the tectonic significance. Journal of African Earth Sciences 141, 49-59.

Aka, F.T., Nagao, K., Kusakabe, M., Sumino, H., Tanyileke, G., Ateba, B., Hell, J., 2004. Symmetrical helium isotope distribution on the Cameroon volcanic line, West Africa. Chemical Geology 203(3), 205-223.

Ateba, B., Dorbath, C., Dorbath, L., Ntepe, N., Frogneux, M., Delmond, J., Manguelle, D., 2009. Eruptive and earthquake activities related to the 2000 eruption of Mount Cameroon volcano (West Africa). Journal of Volcanology and Geothermal Research, 179(3), 206-216.

Ambeh, W., Fairhead, J., Francis, D., Nnange, J., Djallo, S., 1989. Seismicity of the Mount Cameroon region, west Africa. Journal of African Earth Sciences 9(1), 1-7.

Browne, S., Fairhead, J., 1983. Gravity study of the Central African Rift System: A model of continental disruption: 1. The Ngaoundere and Abu Gabra Rifts, Developments in Geotectonics. Elsevier, pp. 187-203.

Burke, K., Dessauvagie, T., Whiteman, A., 1971. Opening of the Gulf of Guinea and geological history of the Benue Depression and Niger Delta. Nature physical science 233(38), 51.

Déruelle, B., Bardintzeff, J.-M., Cheminée, J.-L., Ngounouno, I., Lissom, J., Nkoumbou, C., Étamé, J., Hell, J.-V., Tanyileke, G., N'ni, J., 2000. Eruptions simultanées de basalte alcalin et de hawaiite au mont Cameroun (28 mars–17 avril 1999). Comptes Rendus de l'Académie des Sciences-Series IIA-Earth and Planetary Science 331(8), 525-531.

Déruelle, B., N'ni, J., Kambou, R., 1987. Mount Cameroon: an active volcano of the Cameroon Line. Journal of African Earth Sciences 6(2), 197-214.

Ebinger, C., Sleep N., 1998. Cenozoic magmatism throughout East Africa resulting from impact of a single plume, Nature, 295, 788–791.

Fitton, J., Dunlop, H., 1985. The Cameroon Line, West Africa, and its bearing on the origin of oceanic and continental alkali basalt. Earth and Planetary Science Letters 72(1), 23-38.

Fitton, J., Kilburn, C., Thirlwall, M., Hughes, D., 1983. 1982 eruption of Mount Cameroon, West Africa. Nature 306(12), 327-332

Geiger, H., Barker, A.K., Troll, V.R., 2016. Locating the depth of magma supply for volcanic eruptions, insights from Mount Cameroon. Scientific reports 6, 33629.

Global Volcanism Program, 2013. Cameroon (224010), In: Volcanoes of the World, v. 4.7.0. Venzke, E. (ed.), Smithsonian Institution. Downloaded 25 Jun 2018 (https://volcano.si.edu/volcano.cfm?vn=224010). https://doi.org/10.5479/si.GVP.VOTW4-2013

Gorini, M.A., Bryan, G.M., 1976. The tectonic fabric of Equatorial Atlantic and adjoining continental margins: Gulf of Guinea to northeastern Brazil. Anais da Academia Brasileira de Ciências 48, 101-119.

Halliday, A.N., Dickin, A.P., Fallick, A.E., Fitton, J.G., 1988. Mantle dynamics: a Nd, Sr, Pb and O isotopic study of the Cameroon line volcanic chain. Journal of Petrology 9,181–211.

Halliday, A.N., Davidson, J.P., Holden, P., DeWolf, C.P., Lee, D.C., Fitton, J.G., 1990. Trace element fractionation in plumes and the origin of HIMU mantle beneath the Cameroon Line. Nature 347, 523–528.

Harris, C., Dreyer, T., le Roux, P.J., 2018. *Petrogenesis of peralkaline granite dykes of the Straumsvola Complex, Western Dronning Maud Land, Antarctica*. Contributions to Mineralogy and Petrology, **173 (**8)

Hedberg, J.D., 1968. A Geological analysis of the Cameroon trend. PhD thesis, University of Princeton.

Hildner, E., Klűgel, A., Hauff, F., 2011. Magma storage and ascent during the 1995 eruption of Fogo, Cape Verde Archipelago. Contributions to Mineralogy and Petrology 162, 751–772.

Kamgang, P., Chazot, G., Njonfang, E., Tchoua, F., 2008. Geochemistry and geochronology of mafic rocks from Bamenda Mountains (Cameroon): Source composition and crustal contamination along the Cameroon Volcanic Line. Comptes Rendus Geosciences 340, 850–857.

King, S., Ritsema J., 2000. African hot spot volcanism: Small-scale convection in the upper mantle beneath cratons. Science 290, 1137–1140.

King, S. D., Anderson, D. L., 1995. An alternative mechanism of flood basalt formation, Earth Planetary Science Letters 136, 269–279.

King, S. D., Anderson, D. L., 1998. Edge-driven convection, Earth Planet. Earth Planetary Science Letters 160, 289–296.

Lee, D.C., Halliday, A.N., Fitton, J.G., Poli, G., 1994. Isotopic variations with distance and time in the volcanic islands of the Cameroon line: evidence for a mantle plume origin. Earth and Planetary Science Letters 123, 119–138

Le Bas, M., Le Maitre, R., Streckeisen, A. and Zanettin, B., 1986. A chemical classification of volcanic rocks based on the total alkali-silica diagram. Journal of Petrology 27(3), 745-750.

Lenhardt, N., and Oppenheimer, C., 2014. Volcanism in Africa: Geological perspectives, hazard assessment and societal implications. In: Ismail-Zadeh, A., Urrutia-Fucugauchi, J., Kijko, A., Takeuchi, K., Zaliapin, I. (Eds.) Extreme Natural Hazards, Disaster Risks and Societal Implications, IUGG Special Publication Series 1, Cambridge University Press, 169-199.

Loubser, M., and Verryn, S., 2008. Combining XRF and XRD analyses and sample preparation to solve mineralogical problems. South African Journal of Geology 111(2-3), 229-238.

Marzoli, A., Piccirillo, E., Renne, P., Bellieni, G., Iacumin, M., Nyobe, J. and Tongwa, A., 2000. The Cameroon Volcanic Line revisited: petrogenesis of continental basaltic

magmas from lithospheric and asthenospheric mantle sources. Journal of Petrology, 41(1): 87-109.

Merle, R., Marzoli, A., Aka, F.T., Chiaradia, J., Reisberg, L., Castorina, F., Jourdan, F., Renne, P., N'ni, J., Nyobe, J., 2017. Mt Bambouto Volcano, Cameroon Line: mantle source and differentiation of within-plate alkaline rocks. Journal of Petrology, 58(5): 933-962.

Meyers, J.B., Rosendahl, B.R., Harrison, C.G., Ding, Z.-D., 1998. Deep-imaging seismic and gravity results from the offshore Cameroon Volcanic Line, and speculation of African hotlines. Tectonophysics, 284(1): 31-63.

Moundi A,Wandji P, Bardintzeff J-M, Ménard J-J, Okomo Atouba LC, Mouncherou OF, Reusser E, Bellon H, Tchoua FM., 2007. Les basaltes éocènes à affinité transitionnelle du plateau Bamoun,témoins d'un réservoir mantellique enrichi sous la ligne volcanique du Cameroun. Comptes Rendus Geoscience 339, 396–406

Moreau, C., Regnoult, J.-M., Déruelle, B., Robineau, B., 1987. A new tectonic model for the Cameroon Line, Central Africa. Tectonophysics 141(4), 317-334.

Morgan, W.J., 1983. Hotspot tracks and the early rifting of the Atlantic, Developments in Geotectonics. Elsevier, pp. 123-139.

Ngako, V., Affaton, P., Nnange, J., Njanko, T., 2003. Pan-African tectonic evolution in central and southern Cameroon: transpression and transtension during sinistral shear movements. Journal of African Earth Sciences 36(3), 207-214.

Ngako, V., Njonfang, E., Nnange, J.M., 2006. The North–South Paleozoic to Quaternary trend of alkaline magmatism from Niger–Nigeria to Cameroon: Complex interaction between hotspots and Precambrian faults. Journal of African Earth Sciences 45(3), 241-256.

Njome, M.S., Suh, C.E., Sparks, R.S.J., Ayonghe, S.N., Fitton, J.G., 2008. The Mount Cameroon 1959 compound lava flow field: morphology, petrography and geochemistry. Swiss Journal of Geosciences 101(1), 85-98.

Putirka, K., 1999. Clinopyroxene+ liquid equilibria to 100 kbar and 2450 K. Contributions to Mineralogy and Petrology 135(2-3), 151-163.

Putirka, K., Johnson, M., Kinzler, R., Longhi, J., Walker, D., 1996. Thermobarometry of mafic igneous rocks based on clinopyroxene-liquid equilibria, 0–30 kbar. Contributions to Mineralogy and Petrology 123(1), 92-108.

Putirka, K.D., 2008. Thermometers and barometers for volcanic systems. Reviews in Mineralogy and Geochemistry 69(1), 61-120.

Rankenburg, K., Lassiter, J.C., Brey, G., 2005. The role of continental crust and lithospheric mantle in the genesis of Cameroon Volcanic Line lavas: constraints from isotopic

variations in lavas and megacrysts from the Biu and Jos plateaux. Journal of Petrology 46, 169–190.

Hildner, E., Klűgel, A., Hauff, F., 2011. Magma storage and ascent during the 1995 eruption of Fogo, Cape Verde Archipelago. Contributions to Mineralogy and Petrology (162), 751–772.

Shellnutt, J., Lee, T.Y., Torng, P.K., Yang, C.C., Lee, Y.H., 2016. Late Cretaceous intraplate silicic volcanic rocks from the Lake Chad region: An extension of the Cameroon volcanic line? Geochemistry, Geophysics, Geosystems, 17(7): 2803-2824.

Stracke A., Bizimis M., Salters V. J. M., 2003. Recycling oceanic crust: quantitative constraints. Geochemistry Geophysics Geosyststems 4. doi:10.1029/2001GC000223.

Stroncik, N.A., Klügel, A., Hansteen, T.H., 2009. The magmatic plumbing system beneath El Hierro (Canary Islands): constraints from phenocrysts and naturally quenched basaltic glasses in submarine rocks. Contributions to Mineralogy and Petrology, 157(5): 593.

Suh, C.E., Ayonghe, S., Sparks, R., Annen, C., Fitton, J., Nana, R., Luckman, A., 2003. The 1999 and 2000 eruptions of Mount Cameroon: eruption behaviour and petrochemistry of lava. Bulletin of Volcanology 65(4), 267-281.

Thierry, P., Stieltjes, L., Kouokam, E., Nguéya, P., Salley, P. M., 2008. Multi-hazard risk mapping and assessment on an active volcano: the GRINP project at Mount Cameroon. Natural Hazards 45, 429-456

Toteu, S., 1990. Geochemical characterization of the main petrographical and structural units of Northern Cameroon: implications for Pan-African evolution. Journal of African Earth Sciences 10(4), 615-624.

Toteu, S., Van Schmus, W., Penaye, J., Nyobe, J., 1994. U-Pb and Sm-N edvidence for Eburnian and Pan-African high-grade metamorphism in cratonic rocks of southern Cameroon. Precambrian Research 67(3-4), 321-347.

Wandji, P., Tsafack, J., Bardintzeff, J., Nkouathio, D., Dongmo, A.K., Bellon, H., Guillou, H., 2009. Xenoliths of dunites, wehrlites and clinopyroxenites in the basanites from Batoke volcanic cone (Mount Cameroon, Central Africa): petrogenetic implications. Mineralogy and Petrology 96(1-2), 81-98.

Ngongang, A.W., Lenhardt, N., Smit, A., 2019. Seismic hazard parameter estimation of the Mount Cameroon volcanic region (Cameroon) based on a combination of mixed catalogs. Natural Hazards, 96(1): 369-388.

Yokoyama, T., Kusakabe, M., Nakamura, E., 2007. Plume–lithosphere interaction beneath Mount Cameroon volcano, West Africa: Constraints from ^{238}U–^{230}Th– ^{226}Ra and Sr–Nd–Pb isotope systematics. Geochimica et Cosmochimica Acta 71(7), 1835-1854.

Zindler, A., Hart, S., 1986. Chemical geodynamics. Annual Review of Earth and Planetary Sciences 14(1), 493-571.

Figure captions:

Figure 1: **a**) Topographic map of Mt. Cameroon showing the recent lava flows. The lava flows sampled for this study are 1922, and 1999 eruptions. b) Location of Mt. Cameroon along the Cameroon Volcanic Line.

Figure 2: Microphotographs of clinopyroxene and olivine from the analysed rocks: a) and b) representative textures and zonation patterns of typical clinopyroxene phenocrysts observed in Back-Scattered Electron (BSE) images, c) largely resorbed clinopyroxene as observed under transmitted light, d) clinopyroxene with margin on one side resorbed, e) BSE images of olivine crystals and f) olivine crystal under transmitted light.

Figure 3: Total alkali-silica classification (Le Bas et al., 1986) for the 20th century south-west flank eruptions of Mt. Cameroon. Literature data are from Fitton et al. (1983), Suh et al. (2003), and Yokoyama et al. (2007)

Figure 4: Major element scatter plots for the 20th century south-west flank eruptions of Mt. Cameroon. Literature data are the same as for Fig. 3

Figure 5: Trace element plotted against MgO. Literature data are the same as for Fig. 3

Figure 6: a) $^{87}Sr/^{86}Sr$ vs. $^{143}Nd/^{144}Nd$ isotope diagrams. b) shows the main mantle reservoirs from Zindler and Hart (1986) with all samples plotting within the HIMU mantle reservoir field. c) and d) 1/Sr vs $^{87}Sr/^{86}Sr$ and $^{87}Sr/^{86}Sr$ vs K_2O showing scatter correlations for each eruption, indicating that mixing occurred between magma with slightly different compositions. Literature data are the same as for Fig. 3 and Halliday et al, (1988).

Figure 7: Equilibrium tests and temperature-pressure for clinopyroxene - host rocks in this study. **a**) and b) Mg# of whole rocks against Mg# of respectively analysed clinopyroxene for 1922 and 1999 samples, respectively. c) Temperature (°C) and pressure (kbar) conditions of crystallisation calculated after Putirka, (1996) for clinopyroxenes in equilibrium with their respective host rocks. Mineral/melt Fe/Mg KD values of 0.27±0.03 were used. d) the plot of Nb vs. K_2O showing mixing trends for 1922, 1982, and 1999 lavas. The mixing line of Fitton et al. (1983) for the 1982 and 1959 lavas is also included. Literature data are the same as for Fig. 3

Figure 8: Temporal variations of CaO/Al_2O_3, Rb, La and Rb/Nb, for 1922, 1982 and 1999 lavas of Mount Cameroon

Tables:

Table 1: Whole-rock geochemistry data for the 1922 and 1999 Mount Cameroon lava flows

%	L22A	L22B	L22C	L22D	L22E	L22F	BKB	BKC	BKD	SAMA	BKE	BKF	L99F	L99G
SiO_2	44.04	45.51	42.99	45.24	44.17	43.51	45.37	45.11	45.03	44.42	44.16	43.82	45.56	45.33
TiO_2	3.62	3.23	3.29	3.33	3.56	3.43	3.14	3.14	3.14	3.11	3.10	3.38	3.15	3.15
Al_2O_3	14.04	15.40	11.79	15.11	13.76	14.27	14.66	14.65	14.47	14.90	15.00	14.80	14.74	14.67
Fe_2O_3	13.97	12.15	13.94	12.46	13.99	13.02	12.46	12.45	12.48	13.10	13.40	13.40	12.53	12.50
MnO	0.18	0.17	0.18	0.17	0.18	0.18	0.17	0.18	0.18	0.17	0.17	0.17	0.17	0.18
MgO	6.59	6.66	10.47	6.03	6.88	6.90	6.70	6.56	6.79	6.72	7.01	6.77	6.68	6.72
CaO	12.23	10.71	12.30	10.93	12.19	11.09	11.00	11.14	11.21	10.94	11.35	11.04	11.04	11.25
Na_2O	3.15	4.35	3.03	4.23	3.38	3.31	3.87	3.89	3.83	3.88	3.68	3.88	3.83	3.82
K_2O	1.39	1.68	1.50	1.75	1.28	1.77	1.55	1.55	1.54	1.88	1.68	2.02	1.55	1.57
P_2O_5	0.61	0.89	0.81	0.90	0.59	0.92	0.76	0.75	0.74	0.73	0.71	0.73	0.76	0.75
LOI	0.26	-0.36	-0.26	-0.37	-0.44	0.76	-0.49	-0.47	-0.48	-0.40	-0.39	-0.51	-0.46	-0.51
TOTAL	100.13	99.58	100.12	99.90	99.70	99.34	99.36	99.10	99.08	99.62	100.02	99.64	99.69	99.54
Sc	19.95	16.04	29.74	16.88	20.68	18.12	16.69	18.74	21.52	18.74	19.84	18.58	19.23	19.00
Cr	117.27	75.05	388.76	79.61	123.76	112.19	125.45	139.46	159.77	146.52	191.75	131.19	142.00	157.42
V	322.06	249.24	287.00	259.75	320.57	267.75	255.94	264.21	265.79	272.21	267.47	268.12	270.26	268.31
Ni	67.54	41.00	179.86	46.40	69.00	66.78	75.02	72.01	79.13	79.31	87.06	72.10	77.30	76.20
Co	112.21	67.52	141.89	83.16	93.47	77.00	81.45	79.79	79.03	94.65	81.95	74.34	83.07	72.92
Cu	78.24	65.88	72.75	67.48	79.60	61.81	78.41	81.61	80.67	81.86	82.32	84.02	81.51	79.84
Zn	118.52	111.93	111.85	113.50	117.70	115.39	107.32	109.05	111.11	111.77	108.55	111.27	111.35	108.80
Ga	27	28	24	28	25	23	26	25	25	26	27	25	25	25
Rb	28.68	46.73	35.17	41.61	29.61	45.26	34.26	35.81	42.78	36.56	35.76	36.25	39.03	34.79
Sr	884.12	1080.55	1032.82	1053.03	876.33	1046.59	971.00	995.92	1088.48	1011.18	984.59	1008.22	1033.83	960.28
Y	29.19	32.12	29.97	31.92	28.69	31.61	30.79	30.96	31.89	31.27	30.59	31.19	31.38	30.50
Zr	324.32	430.77	365.87	421.62	316.89	408.06	366.73	366.51	364.79	372.22	359.51	370.49	367.16	360.16
Nb	79.80	115.70	99.46	112.00	7.74	108.37	97.43	96.19	95.54	97.27	93.69	97.18	95.69	93.65
Cs	0.27	0.46	0.36	0.37	0.26	0.45	0.61	0.50	0.54	0.36	0.41	0.40	0.40	0.34
Ba	393.29	534.09	444.57	519.19	384.66	498.89	473.20	463.79	460.94	464.08	449.57	464.77	461.73	448.98
La	58.56	82.50	75.00	79.97	57.32	77.58	72.70	71.81	72.24	72.10	69.83	72.14	71.91	69.46
Ce	117.23	158.89	148.73	155.67	114.82	152.25	142.79	140.58	139.78	141.28	136.66	141.18	140.28	136.96
Pr	14.43	18.66	17.93	18.35	14.11	18.13	17.30	16.95	16.87	16.87	16.45	16.91	16.75	16.29
Nd	55.38	68.83	67.45	68.27	54.34	68.08	64.42	63.66	63.25	63.51	61.79	63.19	62.72	61.20
Sm	10.20	11.77	11.52	11.78	10.05	11.81	11.56	11.27	11.16	11.09	10.96	11.16	11.06	10.80
Eu	3.12	3.50	3.38	3.51	3.04	3.49	3.52	3.43	3.36	3.34	3.32	3.37	3.33	3.26
Gd	8.46	9.24	9.14	9.41	8.42	9.28	8.95	8.99	8.88	9.06	8.76	8.92	8.97	8.81
Tb	1.19	1.27	1.23	1.28	1.15	1.28	1.33	1.31	1.27	1.25	1.23	1.25	1.24	1.21
Dy	6.12	6.68	6.30	6.74	6.08	6.65	6.64	6.49	6.46	6.53	6.34	6.48	6.51	6.32
Ho	1.11	1.20	1.12	1.18	1.08	1.18	1.21	1.25	1.21	1.17	1.19	1.20	1.17	1.14
Er	2.73	2.99	2.79	2.95	2.72	2.91	3.23	3.15	3.12	2.93	3.03	3.04	2.93	2.84
Tm	0.37	0.40	0.37	0.40	0.35	0.39	0.45	0.47	0.44	0.39	0.42	0.42	0.39	0.37
Yb	2.02	2.33	2.10	2.31	1.98	2.26	2.75	2.70	2.55	2.26	2.57	2.61	2.28	2.22
Lu	0.29	0.34	0.30	0.33	0.28	0.32	0.39	0.40	0.36	0.32	0.35	0.35	0.32	0.31
Hf	7.01	8.84	7.85	8.67	6.92	8.57	7.85	7.75	7.67	7.77	7.59	7.70	7.68	7.53
Ta	4.51	6.26	5.37	6.04	4.41	5.90	6.23	5.61	5.44	5.27	5.19	5.33	5.23	5.16
Pb	3.36	5.19	4.27	4.72	3.24	4.72	4.57	4.43	4.68	4.31	4.31	4.33	4.29	4.05
Th	6.03	9.18	7.80	8.71	5.92	8.33	8.11	7.86	8.08	7.84	7.61	7.82	7.95	7.57
U	1.49	2.28	1.95	2.17	1.47	2.10	2.51	2.19	2.08	1.98	2.00	2.03	1.97	1.91
Li	6.25	7.95	6.42	7.72	6.04	7.25	6.73	6.89	7.21	6.74	6.53	6.86	6.98	6.65
$^{87}Sr/^{86}Sr$	0.7033	0.7033	0.7033	0.7033	0.7033	0.7033	0.7031	0.7034	0.7033	0.7033	0.7033	0.7033	0.7033	0.7033
$^{143}Nd/^{144}Nd$	0.5128	0.5128	0.5128	0.5128	0.5128	0.5128	0.5128	0.5128	0.5128	0.5128	0.5128	0.5128	0.5128	0.5128

Table 2: Electron microprobe analyses of clinopyroxene from the 1922 and 1999 lavas

Sample	22C1	22C2	22C3	22C4	22C5	22C6	22C7	22C8	22C9	22C10	22C11	22C12
SiO_2	47.92	47.47	48.28	48.33	49.41	48.11	49.24	50.52	48.43	50.00	49.34	48.96
TiO_2	2.03	2.29	1.85	1.98	1.55	1.55	1.52	1.53	1.82	1.08	1.39	1.69
Al_2O_3	6.48	6.64	5.88	5.95	4.77	4.71	4.76	4.46	5.10	4.14	4.62	4.98
FeO	6.93	7.29	6.83	6.59	5.94	5.91	5.88	5.70	6.12	4.97	5.37	5.63
MnO	0.12	0.07	0.11	0.08	0.09	0.06	0.08	0.09	0.11	0.08	0.05	0.12
MgO	14.27	13.94	14.29	14.22	15.48	16.87	15.84	15.13	14.64	15.69	15.43	15.13
CaO	22.41	22.55	22.72	22.69	22.47	22.23	22.49	22.80	22.87	22.51	22.35	22.48
Na_2O	0.41	0.35	0.38	0.36	0.40	0.46	0.37	0.43	0.39	0.38	0.40	0.40
K_2O	0.01	0.00	0.01	0.01	0.01	0.02	0.02	0.00	0.01	0.01	0.00	0.00
Cr_2O_3	0.27	0.21	0.27	0.20	0.26	0.26	0.22	0.31	0.44	0.85	0.66	0.41
Total	100.85	100.82	100.62	100.41	100.37	100.16	100.42	100.97	99.92	99.71	99.61	99.78
Mg#	78.60	77.33	78.85	79.37	82.29	83.58	82.77	82.54	81.02	84.92	83.67	82.74

Sample	22E1	22E2	22E3	22E4	22E5	22E6	22E7	22 E8	22E9	22E10	22E11	22E12
SiO_2	48.45	48.52	47.10	47.32	50.98	50.18	50.17	50.31	45.83	45.68	46.97	46.84
TiO_2	1.87	1.81	2.13	2.23	1.09	1.23	1.29	1.23	2.83	2.82	2.47	2.40
Al_2O_3	5.27	5.08	6.30	6.27	3.52	4.10	4.15	4.15	7.55	7.46	6.69	6.44
FeO	6.52	6.20	7.26	6.93	5.18	5.34	5.42	5.40	7.43	7.19	6.94	6.94
MnO	0.11	0.05	0.13	0.08	0.11	0.08	0.07	0.10	0.13	0.07	0.11	0.07
MgO	14.35	14.70	13.74	13.65	15.99	15.63	15.64	15.52	13.00	13.15	13.43	13.76
CaO	22.50	22.59	22.50	22.53	22.08	22.17	22.26	22.24	22.64	22.54	22.47	22.39
Na_2O	0.44	0.38	0.37	0.39	0.36	0.37	0.37	0.36	0.50	0.54	0.50	0.45
K_2O	0.01	0.01	0.02	0.01	0.02	0.02	0.00	0.00	0.01	0.01	0.02	0.01
Cr_2O_3	0.32	0.30	0.11	0.12	0.41	0.59	0.61	0.56	0.01	0.02	0.00	0.07
Total	99.84	99.63	99.64	99.55	99.74	99.69	99.98	99.88	99.92	99.48	99.62	99.37
Mg#	79.70	80.88	77.15	77.83	84.61	83.93	83.73	83.67	75.72	76.52	77.52	77.95

Sample	99F1	99F2	99F3	99F4	99F5	99F6	99F7	99F8	99F9	99F10	99F11	99F12
SiO_2	47.71	47.75	47.13	46.88	48.62	48.29	48.27	46.02	50.79	50.89	50.74	50.51
TiO_2	1.95	2.11	2.34	2.36	1.88	1.80	1.77	2.75	1.09	1.10	1.11	1.25
Al_2O_3	5.82	6.20	6.69	7.11	5.37	5.31	5.24	7.19	4.12	3.97	4.05	4.22
FeO	6.73	6.68	7.05	7.18	6.14	6.07	5.77	7.30	4.95	5.12	5.11	5.27
MnO	0.06	0.12	0.13	0.11	0.08	0.13	0.06	0.10	0.14	0.14	0.15	0.13
MgO	14.24	14.02	13.75	13.73	14.68	14.48	14.47	13.28	15.85	16.02	16.00	15.82
CaO	22.27	22.39	22.17	22.38	22.70	22.72	22.68	22.34	22.49	22.52	22.59	22.43
Na_2O	0.45	0.43	0.47	0.42	0.43	0.39	0.41	0.46	0.36	0.36	0.41	0.35
K_2O	0.03	0.02	0.01	0.01	0.02	0.01	0.00	0.00	0.01	0.01	0.00	0.00
Cr_2O_3	0.22	0.29	0.13	0.20	0.27	0.37	0.50	0.06	0.49	0.42	0.52	0.52
Total	99.47	99.99	99.85	100.36	100.18	99.56	99.17	99.50	100.28	100.55	100.68	100.49
Mg#	79.06	78.92	77.67	77.32	80.99	80.97	81.73	76.42	85.10	84.80	84.80	84.25

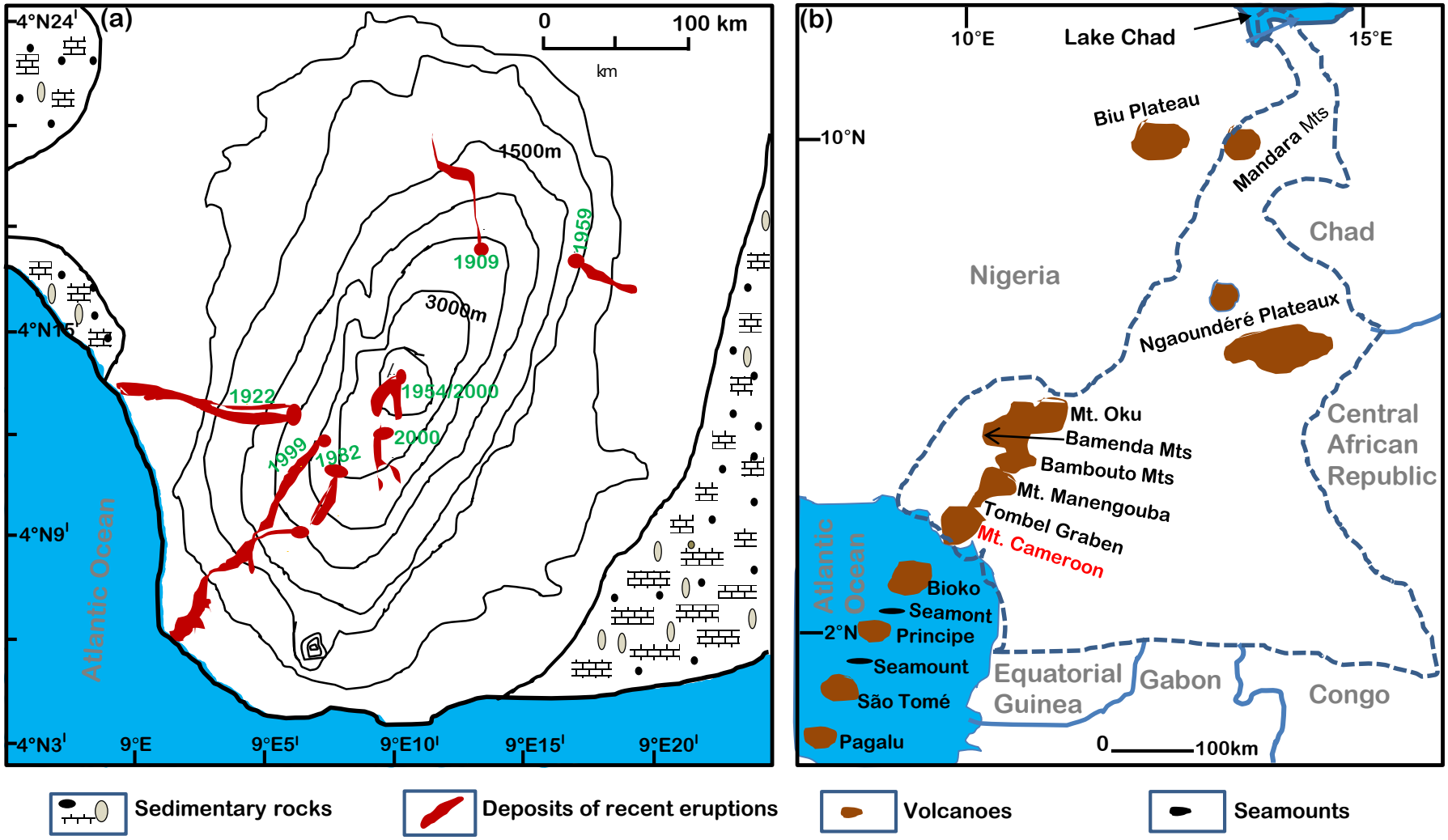

Figure 1: **a**) Topographic map of Mt. Cameroon showing the recent lava flows. The lava flows sampled for this study are 1922, and 1999 eruptions. b) Location of Mt. Cameroon along the Cameroon Volcanic Line.

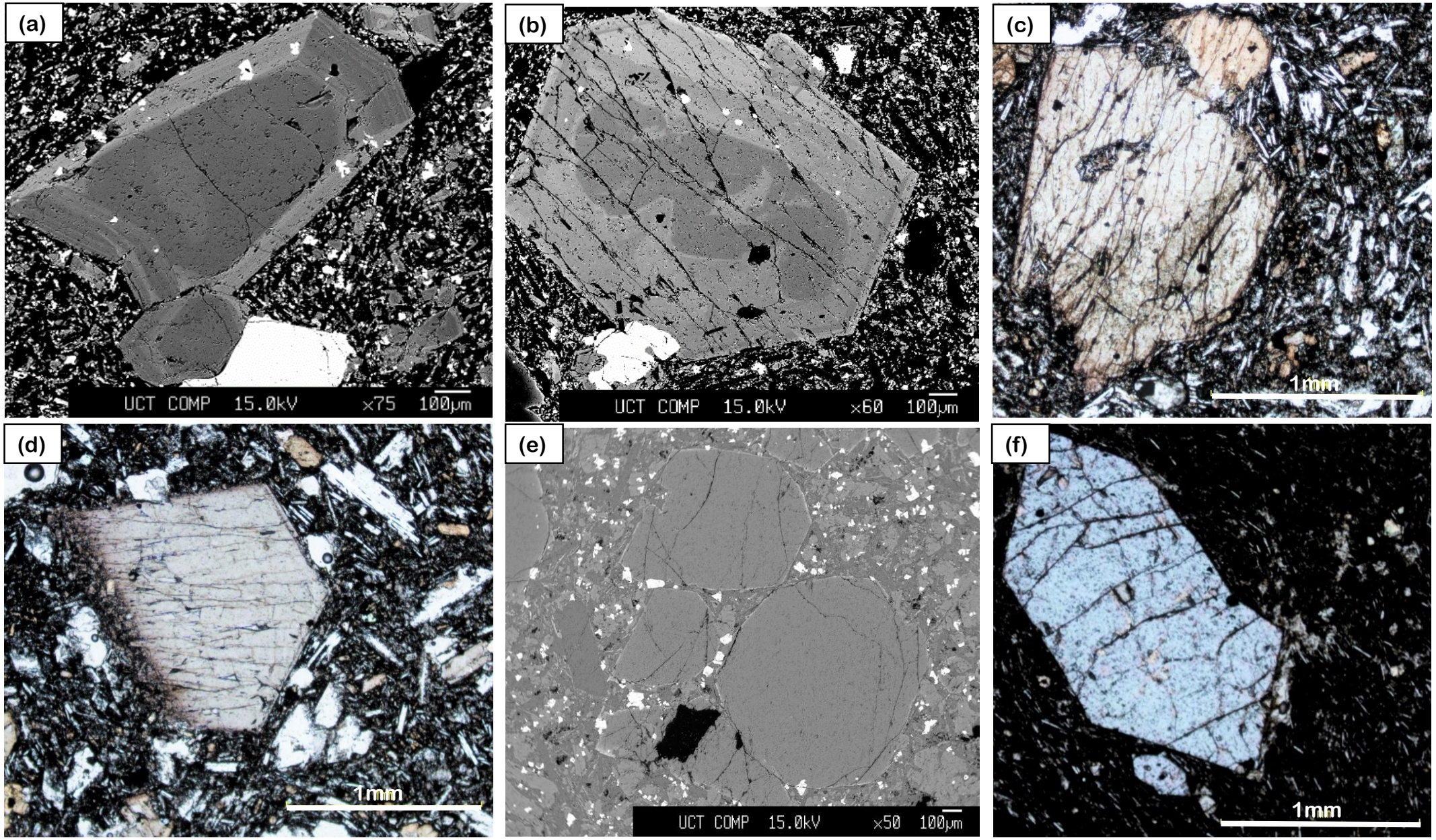

Figure 2: Microphotographs of clinopyroxene and olivine from the analysed rocks: a) and b) representative textures and zonation patterns of typical clinopyroxene phenocrysts observed in Back-Scattered Electron (BSE) images, c) largely resorbed clinopyroxene as observed under transmitted light, d) clinopyroxene with margin on one side resorbed, e) BSE images of olivine crystals and f) olivine crystal under transmitted light.

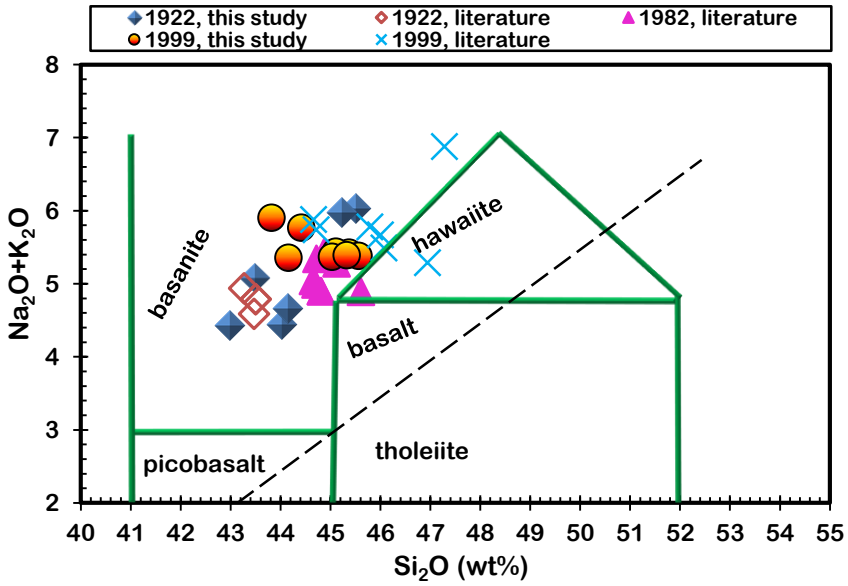

Figure 3: Total alkali-silica classification (Le Bas et al., 1986) for the 20th century south-west flank eruptions of Mt. Cameroon. Literature data are from Fitton et al. (1983), Suh et al. (2003), and Yokoyama et al. (2007)

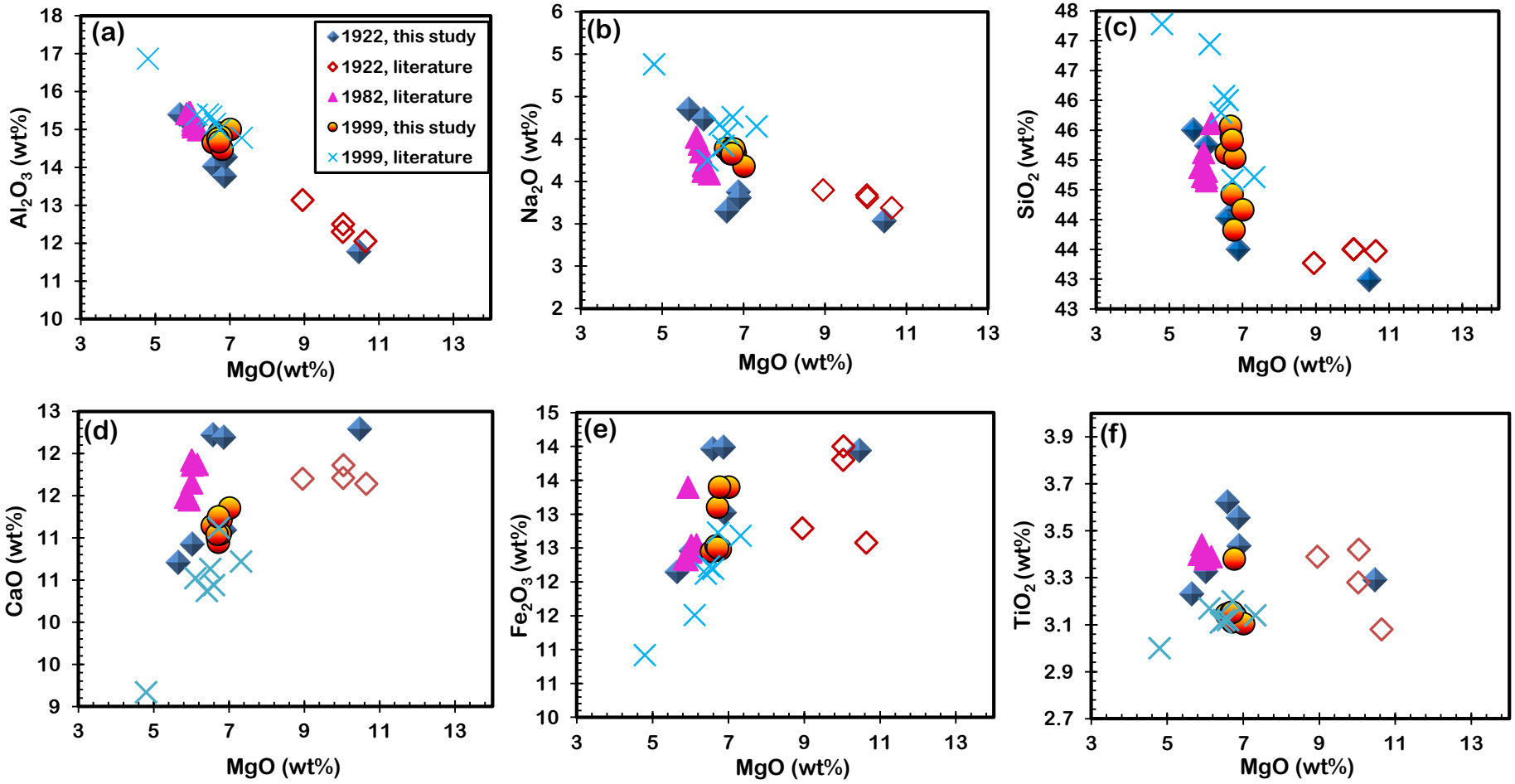

Figure 4: Major element scatter plots for the 20th century south-west flank eruptions of Mt. Cameroon. Literature data are the same as for Fig. 3

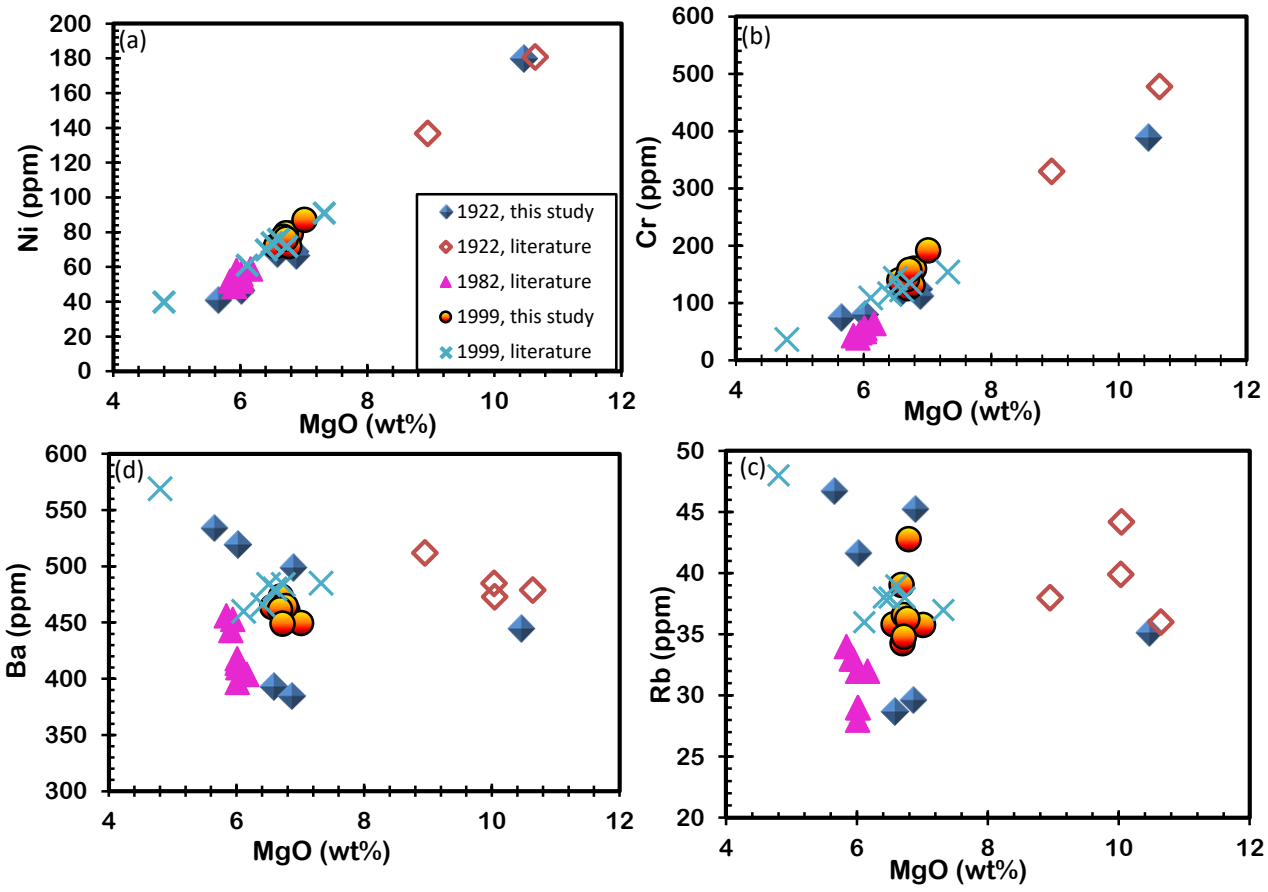

Figure 5: Trace element plotted against MgO. Literature data are the same as for Fig. 3

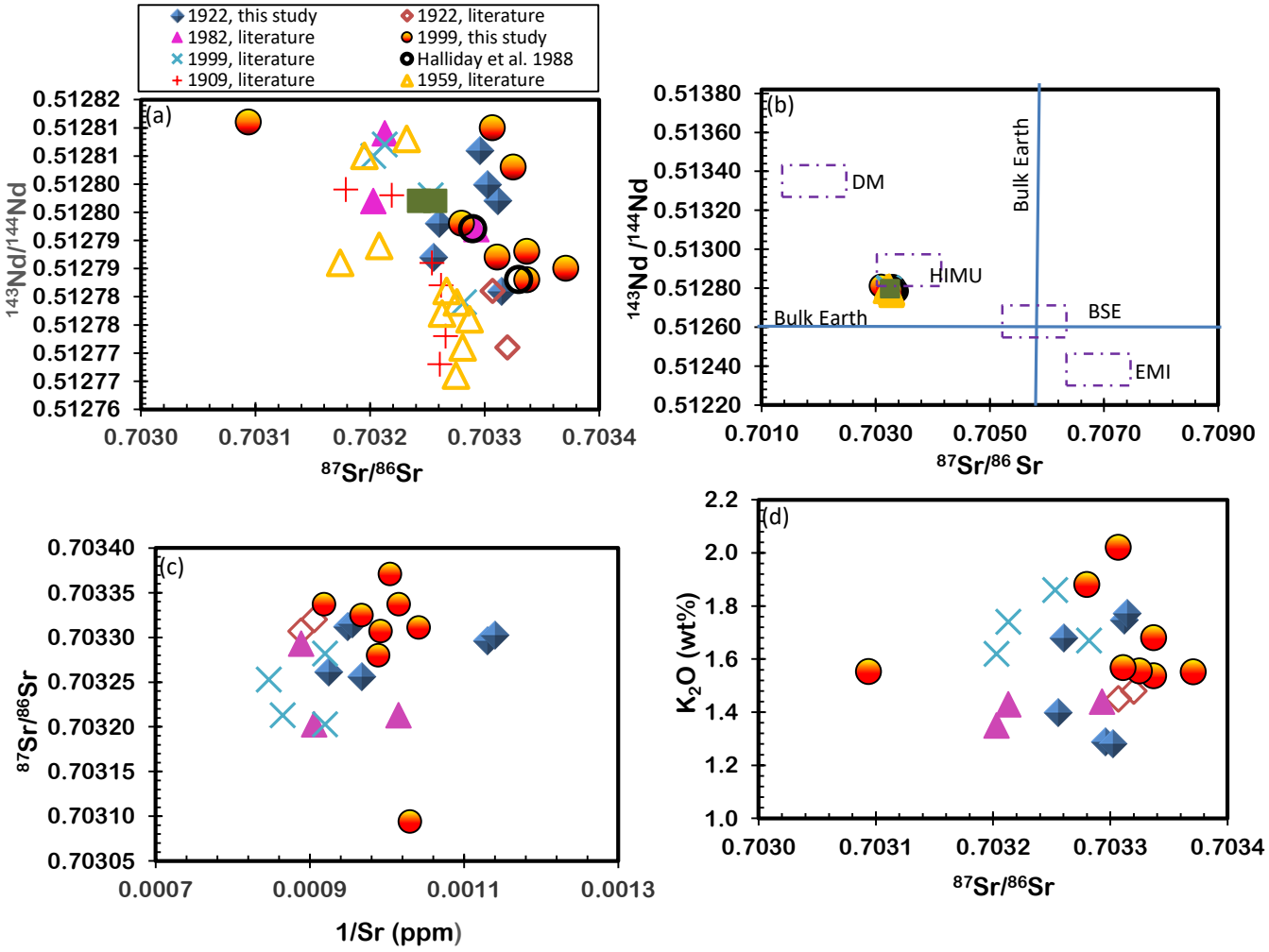

Figure 6: a) $^{87}Sr/^{86}Sr$ vs. $^{143}Nd/^{144}Nd$ isotope diagrams. b) shows the main mantle reservoirs from Zindler and Hart (1986) with all samples plotting within the HIMU mantle reservoir field. c) and d) 1/Sr vs $^{87}Sr/^{86}Sr$ and $^{87}Sr/^{86}Sr$ vs K_2O showing scatter correlations for each eruption, indicating that mixing occurred between magma with slightly different compositions. Literature data are the same as for Fig. 3 and Halliday et al, (1988).

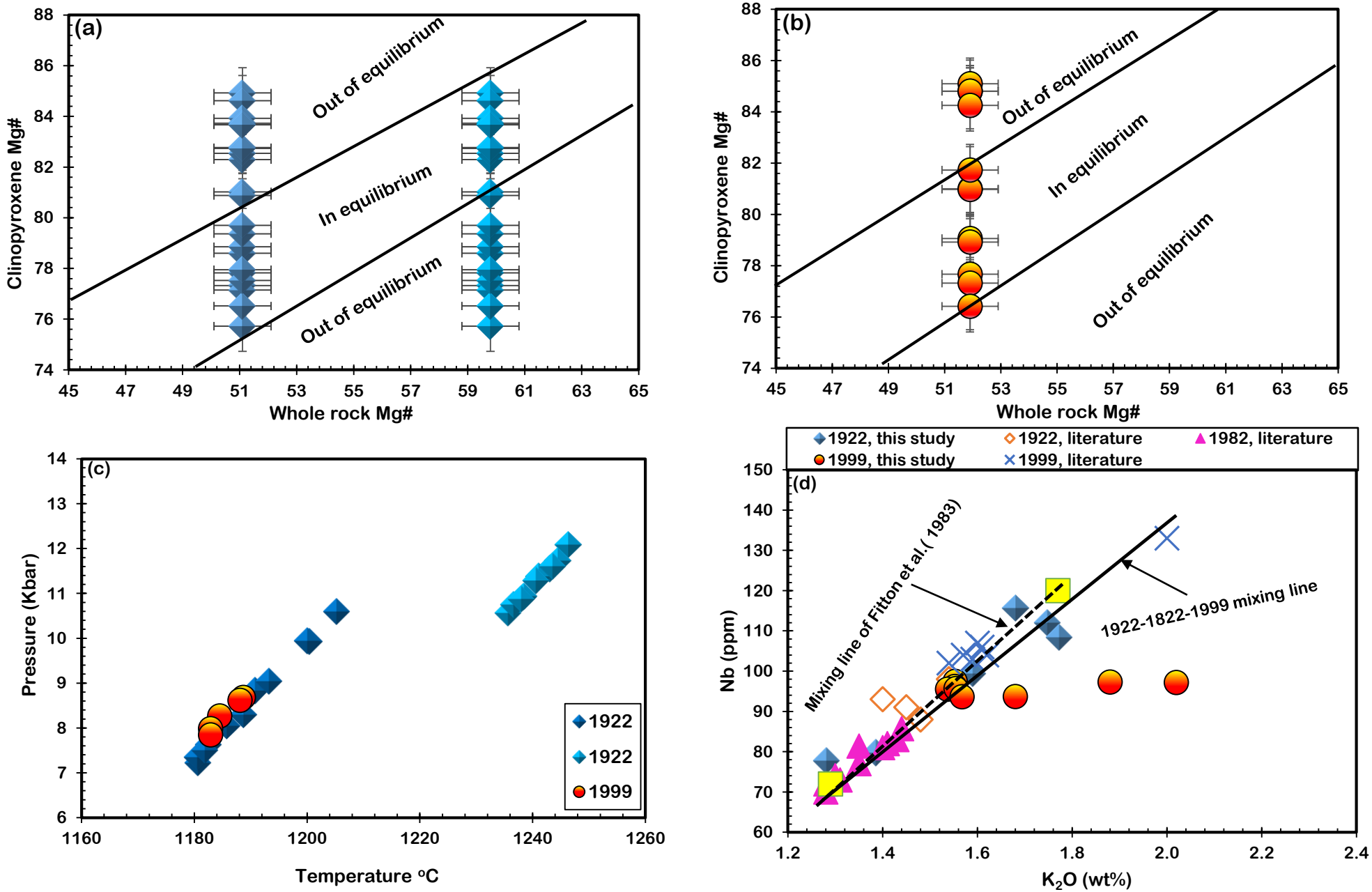

Figure 7: Equilibrium tests and temperature-pressure for clinopyroxene - host rocks in this study. **a**) and b) Mg# of whole rocks against Mg# of respectively analysed clinopyroxene for 1922 and 1999 samples, respectively. c) Temperature (°C) and pressure (kbar) conditions of crystallisation calculated after Putirka, (1996) for clinopyroxenes in equilibrium with their respective host rocks. Mineral/melt Fe/Mg KD values of 0.27±0.03 were used. d) the plot of Nb vs. K_2O showing mixing trends for 1922, 1982, and 1999 lavas. The mixing line of Fitton et al. (1983) for the 1982 and 1959 lavas is also included. Literature data are the same as for Fig. 3

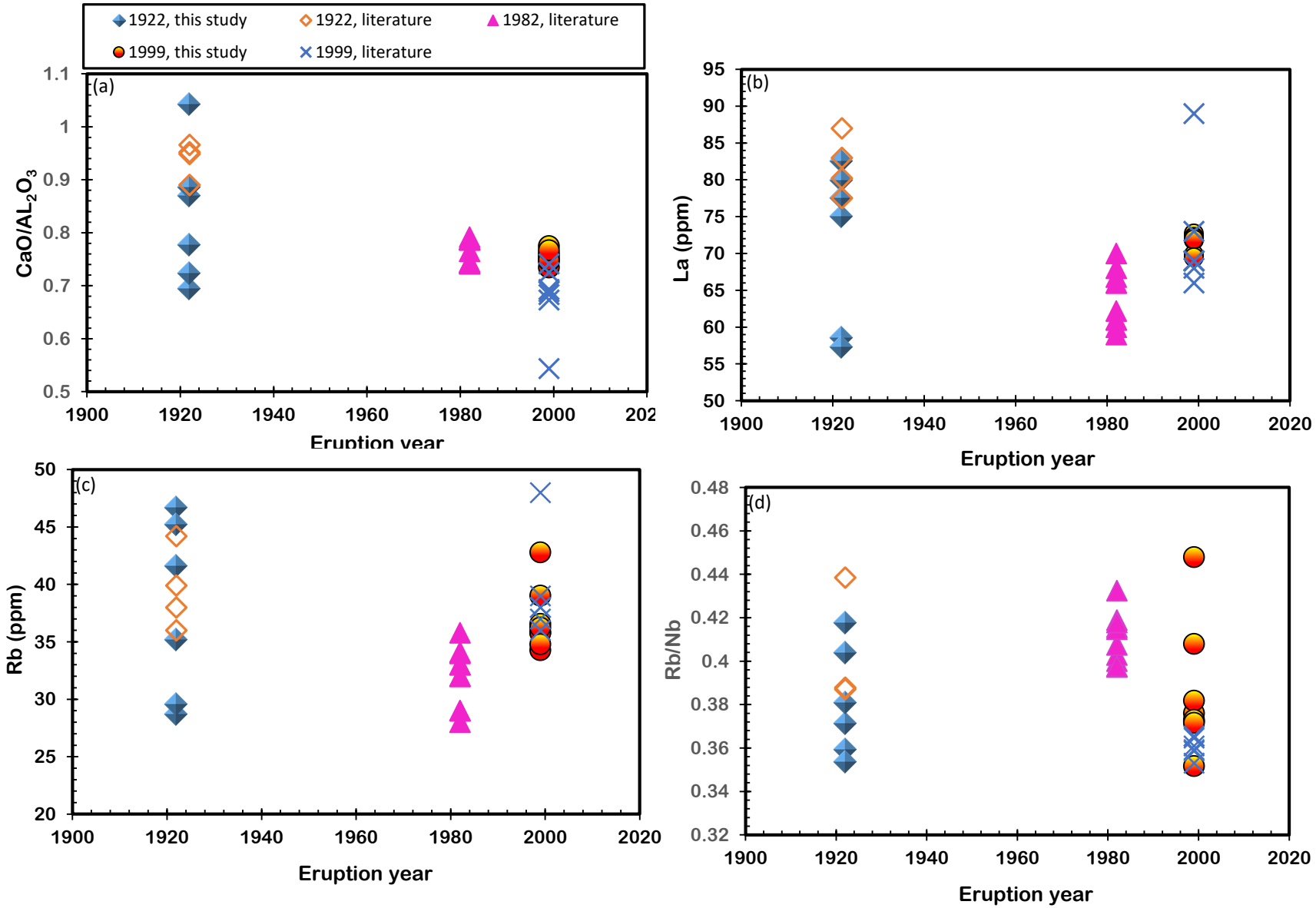

Figure 8: Temporal variations of CaO/Al_2O_3, Rb, La and Rb/Nb, for 1922, 1982 and 1999 lavas of Mount Cameroon